

Analysis of laser radiation transmitted through a plasma as a method for estimating the internal parameters of the laser-produced plasma

© P.S. Butorin¹, A.V. Belashov¹, S.G. Kalmykov¹, M.E. Sasin¹, P.Yu. Serdobintsev^{2,3}

¹ Ioffe Institute,
197101 St. Petersburg, Russia

² Peter the Great Saint-Petersburg Polytechnic University,
197101 St. Petersburg, Russia

³ St. Petersburg State University,
199034 St. Petersburg, Russia

e-mail: butorin_ps@mail.ioffe.ru

Received August 15, 2023

Revised December 11, 2023

Accepted December 18, 2023

A technique is described that makes it possible to obtain the distribution of the absorbed energy of a laser pulse over the cross section of the laser-produced plasma. The infrared laser radiation that creates the plasma at the same time plays the role of radiation that probes it. The pattern of the absorbed energy distribution over the beam section is increased to macroscopic dimensions, that allows to study it using standard methods. As a result, spatial resolution within the plasma location of several units/tens of microns has been attained. The data on the distribution of the laser energy absorbed part over the plasma cross section give an idea about the characteristic features of the distribution of the plasma temperature.

Keywords: laser spark, laser, radiation absorption, laser plasma parameters, infrared radiation.

DOI: 10.61011/EOS.2023.12.58180.5493-23

Introduction

The present work is a part of the studies of the plasma generated by a laser beam on a Xe gas-jet target that are being performed at the Ioffe Institute since 2014 [1–3]. In them, such a plasma is considered as the source of working radiation in the EUV (Extreme UltraViolet) range for nanolithography. The motivation for this research was a suggestion made in 2013 at the Institute for Physics of Microstructures (IPM) of the Russian Academy of Sciences about a possible branch of lithography with a wavelength of about 11 nm [4,5]. In this case, one could use a source with the plasma of Xe, the emission intensity of which at $\lambda \approx 11$ nm is almost an order of magnitude higher than that at $\lambda = 13.5$ nm (the wavelength used in the contemporary lithography). Such a source would be „clean“, debrisless, relatively simple and cheap compared to the laser-plasma source applied in the industrial lithography, in which a jet of tin microdroplets is used as a target to achieve higher EUV radiation intensity [6].

The initial goal of the research at the Ioffe Institute was to raise the efficiency of the EUV source to a level acceptable in the industrial nanolithography. As a result, the record to date efficiency of the Xe laser-plasma source in converting the laser light into the radiation with $\lambda = 11.4$ nm has been demonstrated: $CE \approx 4\%$ [7]. Also, a similar conversion efficiency for the same source, but under different experimental conditions was observed in the IPM [8] at $\lambda = 10.8$ nm: $CE = 1.8\%$.

Jointly performed measurements of the energy emitted by the plasma within the EUV range and the laser radiation energy absorbed in it as a function of the plasma size (i.e., the laser beam diameter) [7,9] showed an expressed similarity of these two functions, with maxima of both the absorption and the emission being observed when a dense part of the gas jet was irradiated with a wide laser beam ($\varnothing_{\text{las}} \approx 400 \mu\text{m}$). If the target was in focus ($\varnothing_{\text{las}} \approx 50 \mu\text{m}$), i.e., at the highest laser beam power density ($\approx 2 \text{ TW/cm}^2$), the values of both quantities were the smallest, with the maxima exceeding the minima by 5–10 times. The reason for such an increase in absorption/emission with increasing size of the laser-plasma formation was explained on the basis of the hypothesis of hydrodynamic outflow of the plasma outwards the laser-irradiated region, that leads to reducing the lifetime of the dense absorbing and actively emitting plasma formation. At this, the larger the laser beam diameter is, the longer is the lifetime of plasma created by it. This dependence exists as long as the intensity of the laser radiation is not too low (insufficient for plasma excitation and heating).

It was also shown in [9] that measurements of the absorption of the infrared (IR) laser radiation in a laser plasma can be considered as a method for estimating internal plasma parameters such as temperature and mean ion charge. Note, that until now in experiments it has been possible to study only the radiation of such a plasma. However, the nonequilibrium and the absence of discrete lines in the spectra of the dense laser plasma of multielectron

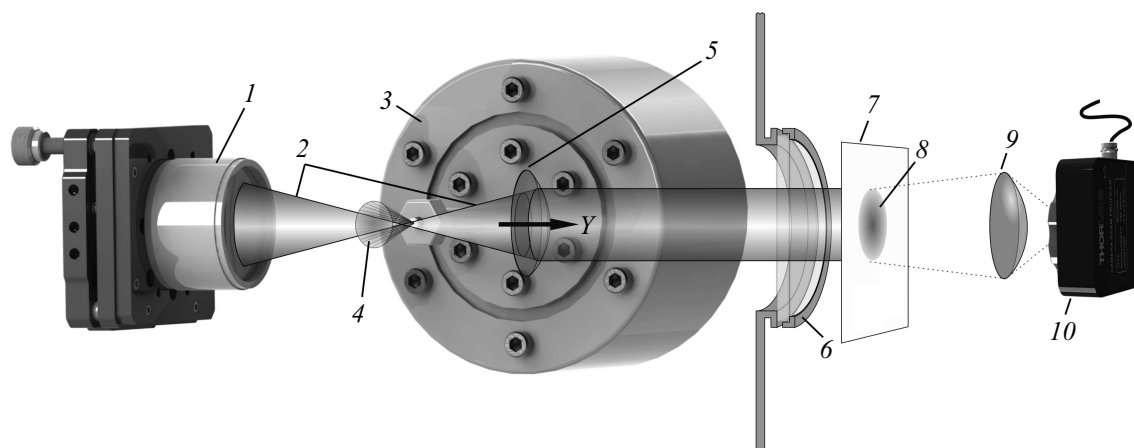


Figure 1. Scheme of the experimental setup. (1) — focusing lens, (2) — Nd:YAG laser beam, (3) — gas-jet target generator, (4) — supersonic Xe microjet, (5) — the lens converting the diverging laser beam into the parallel one, (6) — the glass window of the vacuum chamber, (7) — scattering screen, (8) — the image of the beam cross section on the screen, (9) — the lens to transfer the image to a CCD matrix, and (10) — the CCD sensor.

ions [10] made standard spectroscopic diagnostic methods inapplicable [11,12].

Unlike [9], where only the integral measurements over space and time are discussed, this work is devoted to studying the absorption structure with high spatial resolution. The laser beam passing through the plasma and partially absorbed by it carries an information about the absorption distribution over the plasma cross-section. In this sense, the laser radiation probes the plasma in much the same way as X-rays do in fluoroscopy. Unlike the fluoroscopy, the probing radiation of the optical IR range is used in the „IR-scopy“. It can be easily converted with the conventional refractive optics. In particular, the pattern of the absorption distribution over the cross section, which has a diameter of the order of tens to hundreds of micrometers within the area where the beam passes through the plasma, is enlarged to macroscopic dimensions of the order of a few millimeters and can be studied with standard methods (e.g., with recording on a CCD array). In the case, when the laser plasmas have diameter of approximately $50\ \mu\text{m}$ (the case of sharp focusing the beam on the jet axis), the space resolution of the details of the absorption pattern is limited by the diffraction limit, which is $1\text{--}2\ \mu\text{m}$ for the Nd:YAG laser radiation ($\lambda = 1.064\ \mu\text{m}$).

Experimental setup

The measurements were carried out on an installation schematically shown in Fig. 1

In all performed experiments, the generator of radiation creating the plasma was a multimode Nd:YAG laser ($\lambda = 1.064\ \mu\text{m}$) with pulse energy $E_{\text{las}} = 1\text{--}1.4\ \text{J}$ and duration $\tau_{\text{las}} \approx 10\ \text{ns}$ (FWHM — full width at half maximum). At the laser output window, the beam diameter was $\Phi_{\text{las}} = 8\text{--}10\ \text{mm}$ and its divergence was $\theta_{\text{las}} = 1.5\ \text{mrad}$. Then the beam passed through a telescope-expander, which

increased its diameter to $\Phi_{\text{expand}} = 26\text{--}29\ \text{mm}$, and the divergence, accordingly, decreased to $\theta_{\text{expand}} = 0.5\ \text{mrad}$. The expanded beam was introduced into the vacuum chamber through a window and then focused onto the target using a specially designed aberration-free lens with focal length $F_{\text{lens}} = 82\ \text{mm}$. The target was a pulsed axisymmetric supersonic Xe microjet flowing from a Laval nozzle (critical diameter — $0.2\ \text{mm}$, exit diameter — $1.1\ \text{mm}$, length — $13\ \text{mm}$) into vacuum. The axes of the jet and the laser beam (Y) intersected at a right angle. In all the experiments described, the intersection point was located at a distance of $1\ \text{mm}$ from the nozzle exit. Gas pulses were synchronized with laser pulses so that the latter were induced when a quasi-stationary jet flow regime was established. The Xe density distributions along the radius and length of the gas-jet target were calculated for various experimental conditions using numerical simulations [13,14].

Figure 2, (a) shows the radial distribution of the concentration of Xe atoms in the target under the conditions of the present work. The typical background pressure of residual gas in the vacuum chamber was $\approx 10^{-4}\ \text{mm Hg}$. The jet generator was mounted on a positioner, which allowed the nozzle to be moved from pulse to pulse in all three coordinates relative to a fixed focus position with an accuracy of $5\ \mu\text{m}$. When the nozzle was moved along the laser beam axis (Y), the distance between the jet axis and the focus changed, and the diameter of the beam at its intersection with the jet changed accordingly (Fig. 2, (b) and [15]). In the area of intersection of the laser beam axis with the axis of the gas jet, plasma appeared.

A lens mounted inside the vacuum chamber converted the beam diverging beyond the focus (both with and without plasma) into a parallel one, which was output from the chamber through a window and directed to a scattering screen. The image of its cross-section on the screen was transferred with the help of another lens to a CCD matrix

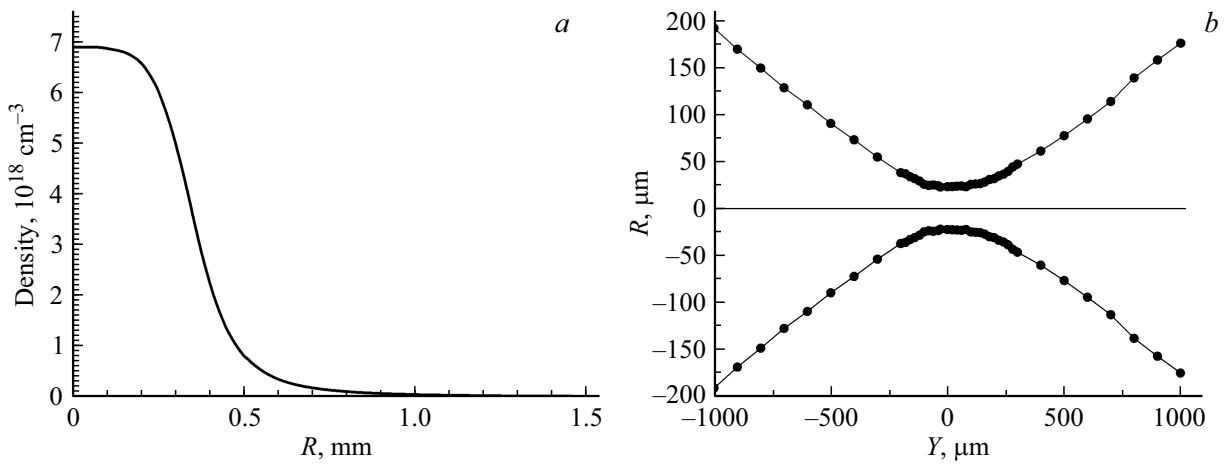


Figure 2. (a) The radial distribution of the concentration of Xe atoms in the target jet at the distance of 1mm from the nozzle exit and at the pressure $P_0 = 13$ atm before the nozzle entrance. The point $R = 0$ is located on the jet axis. (b) Effective radius of the laser beam as a function of coordinate Y (along the beam axis). Black dots represent the effective beam radii measured using the photosensitive CCD matrix.

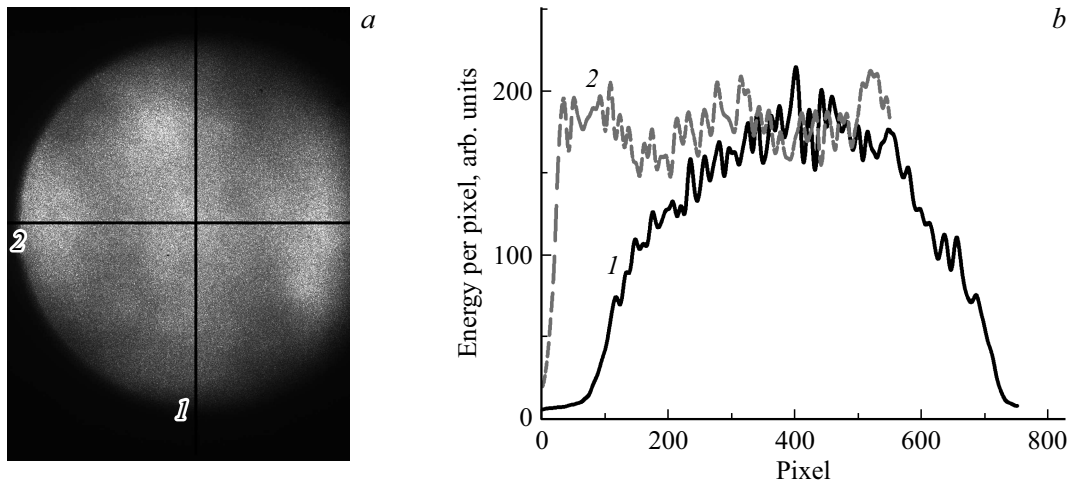


Figure 3. (a) Energy distribution over the cross section of the IR laser beam as recorded with the CCD sensor; (b) distributions along two mutually perpendicular diameters: the vertical diameter (1) and the horizontal one (2).

(BC106-M beam profiler produced by Thorlabs Inc., USA). This instrument has a spatial resolution (i.e., CCD pixel size) of $6\mu\text{m}$ and allows studies of beams with diameters from $30\mu\text{m}$ and more.

Distributions of energy density over the beam cross section for both the beam passed through the plasma (W_{tr}) and the beam that passed through the vacuum with no plasma (W_0) were recorded and then were compared making it possible to determine the density of energy absorbed by the plasma, $W_{abs} = W_0 - W_{tr}$.

Results

The distributions recorded on the CCD were averaged over 15–20 pulses to eliminate their pulse-to-pulse variations. A typical averaged distribution for pulses without the plasma is shown in Fig. 3(a). The inhomogeneity of

the distribution seen in this figure is due to the multi-mode structure of the laser beam.

Measurements when the beam passed through the plasma were carried out at 6 positions of the gas-jet target on the beam axis: $Y = 0$ (in the geometric focus), 200, 400, 600, 800, and $1000\mu\text{m}$. The resulting distributions of the absorbed energy density, W_{abs} , for all six cases are presented in Fig. 4.

The distributions of the relative fraction of absorbed energy, W_{abs}/W_0 , are given in Fig. 5. In all fragments of this Figure, there is a lighter annular area at the edge of the plasma, which looks like a zone with higher absorption. However, the most plausible explanation is the refraction of the IR radiation at the plasma boundary where its density gradient is greatest. The refraction index of electromagnetic waves in plasma, a medium with free electrons, is $n < 1$. Therefore, the convex surface of the plasma formation,

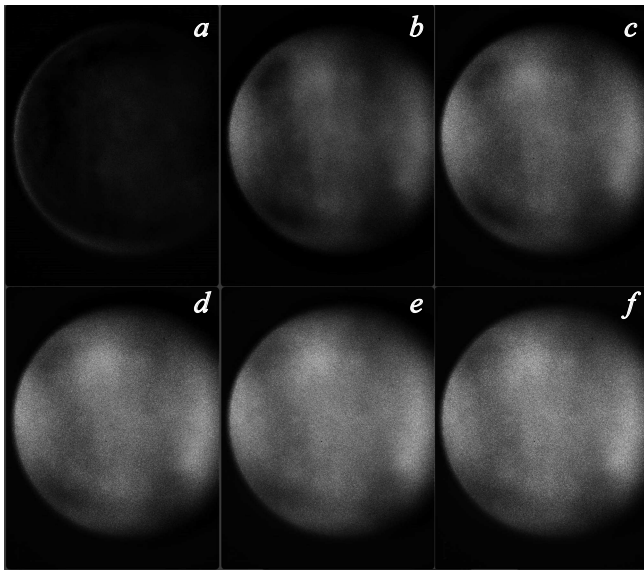


Figure 4. Distribution of the absorbed energy density, $W_{\text{abs}} = W_0 - W_{\text{tr}}$, over the laser beam cross section for: (a) — $Y = 0$, (b) — $Y = 200 \mu\text{m}$, (c) — $Y = 400 \mu\text{m}$, (d) — $Y = 600 \mu\text{m}$, (e) — $Y = 800 \mu\text{m}$, (f) — $Y = 1000 \mu\text{m}$.

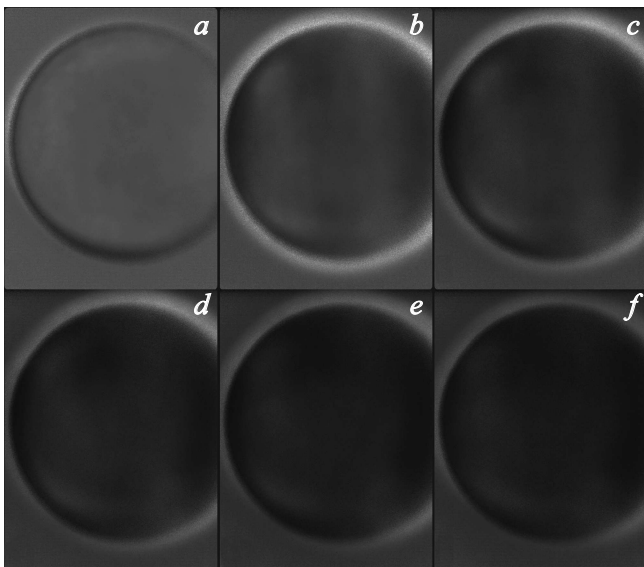


Figure 5. Distributions over the cross section of the fraction of absorbed laser energy, W_{abs}/W_0 , for (a) — $Y = 0$, (b) — $Y = 200 \mu\text{m}$, (c) — $Y = 400 \mu\text{m}$, (d) — $Y = 600 \mu\text{m}$, (e) — $Y = 800 \mu\text{m}$, (f) — $Y = 1000 \mu\text{m}$.

in contrast to the glass lens with $n > 1$, defocuses the light beam and removes the radiation from the peripheral zone outwards the aperture of the receiving optics, thereby simulating increased absorption. In the remaining, inner part of the beam, the distribution of the absorbed fraction is quite uniform (Fig. 6). This figure shows the local absorbed fraction values at various points in the beam cross section for three target positions on axis Y .

To conclude this section, note that processing of the primary CCD images (such as those shown in Fig. 3 (a)) was performed using the Matlab software suit.

Discussion and conclusion

The local values of the absorbed fraction above are in good agreement with those integrated over the beam cross section [9]. In the both studies, the relative fraction of the laser radiation absorbed in the plasma is $\approx 10\%$ at sharp beam focusing on the jet axis ($Y = 0$) and about 65% for the wide defocused beam (e.g., at $Y = 1000 \mu\text{m}$).

As is known from the theory of electromagnetic wave propagation in plasma, the absorption coefficient can be expressed in terms of plasma parameters [16],

$$\mu = \frac{4\pi e^2 n_e v_{ei}}{m_e c \omega^2} = \frac{4\pi e^2 n_e n_i \langle \sigma_{ei} v_e \rangle}{m_e c \omega^2} = \frac{16\pi^2 e^6 L_C n_i^2 \langle Z \rangle^3}{(3m_e)^{3/2} c \omega^2 (k_B T)^{3/2}}, \quad (1)$$

where n_i is the concentration of plasma ions equal to the concentration of gas atoms, $n_e = \langle Z \rangle n_i$ is the concentration of electrons, $\langle Z \rangle$ is the mean ion charge, v_{ei} is the frequency of electron-ion collisions, σ_{ei} is the Coulomb collision cross section, T_e is the temperature of electrons, v_e is their thermal velocity, $\langle \sigma_{ei} v_e \rangle$ is averaging over the velocity ensemble, L_C is the Coulomb logarithm, k_B is the Boltzmann constant, ω is the angular frequency of laser radiation, e and m_e are the electron charge and mass, and c is the speed of light.

To realize the „diagnostic potential“ of the absorption measurements accordingly to that described in [9], it is necessary, first, to determine absorption coefficient, μ , from the experimental data. Its value averaged over an effective absorption length in plasma, L_{pl} , is derived with the help of the relation $W_{\text{tr}}/W_0 = 1 - W_{\text{abs}}/W_0 = \exp(-\mu L_{pl})$. On the other hand, values of μ at different plasma temperatures are calculated using Eq. (1). Mean ion charge, $\langle Z \rangle$, in the latter is also determined as a function of temperature (at a given plasma density) by means of the method in [9] developed especially for nonequilibrium short-lived plasmas. Comparing the experimental value of μ with the calculated ones, one can estimate both T and $\langle Z \rangle$.

To implement the diagnostic approach the mechanism of which was described in detail in [9], one needs to determine absorption coefficient μ from the experimental data. For the measured W_{abs}/W_0 ratio, the value of μ averaged over the effective absorption length in plasma L_{pl} is derived from relation At the same time, it is possible to obtain the calculated value of $\mu(T)$ at different plasma temperatures by supplementing Eq. (1) with the method (developed and described in [9]) for calculating the mean ionic charge of nonequilibrium short-lived plasma, which relates parameters T and $\langle Z \rangle$. Comparing the experimental value of μ with the calculated value, one can then estimate both T and $\langle Z \rangle$.

Thus, the homogeneity of the spatial distribution of the absorption (Fig. 6) ultimately testify to the homogeneity of

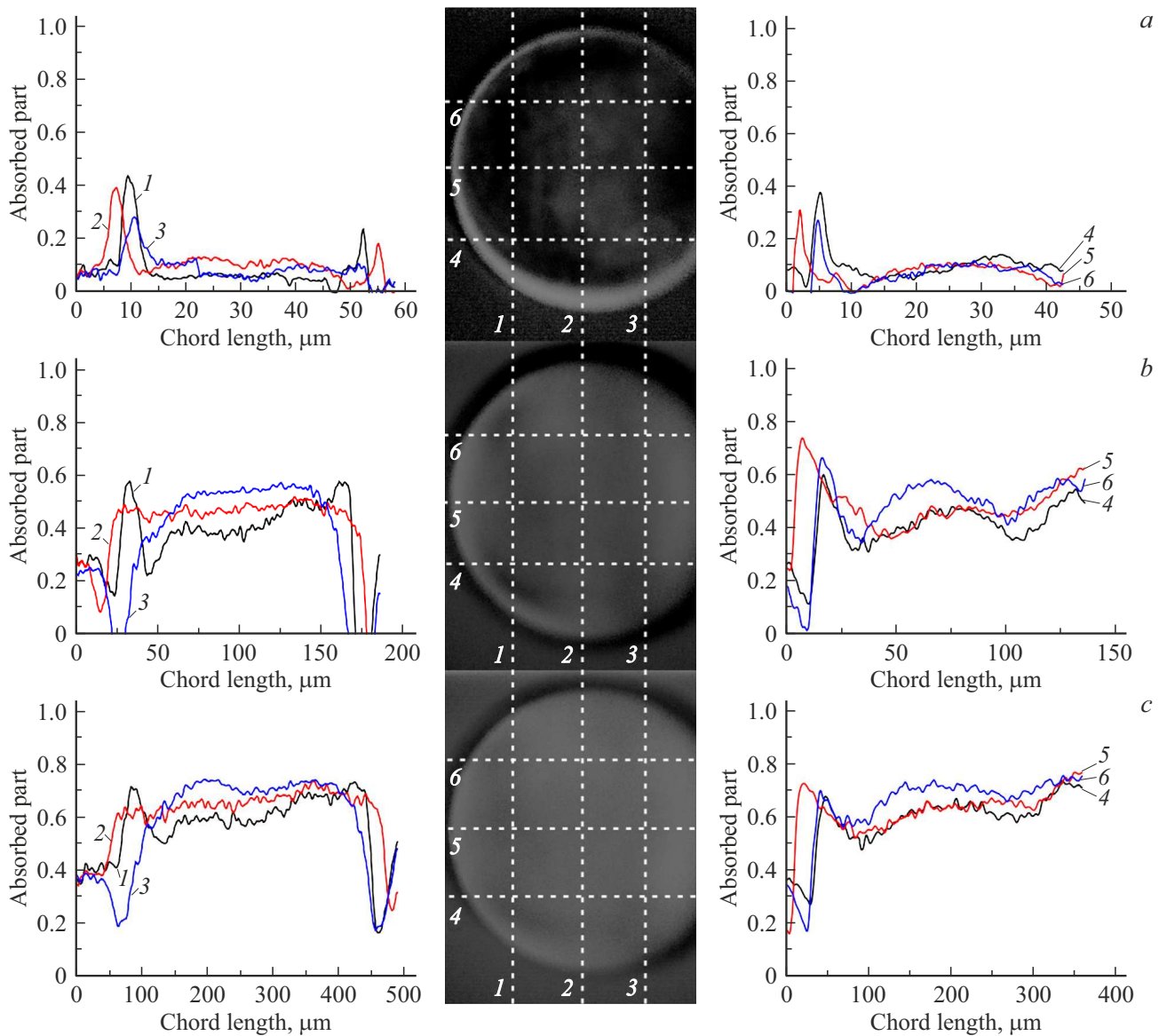


Figure 6. The distributions of the absorbed fraction along three vertical chords (chord numbers are 1, 2, and 3) are shown on the left side of the Figure, and the distributions along three horizontal chords (chord numbers are 4, 5, and 6) can be seen on the right. The arrangement of the chords against the background of the entire cross section can be seen in the middle part of the Figure. The distributions of the absorbed fraction are given for three experimental cases, when the gas-jet target was located at the focus of the laser beam ($Y = 0$, case (a)), and also at distances of $Y = 400 \mu\text{m}$ (b) and $Y = 1000 \mu\text{m}$ (c) from it along the beam axis.

the temperature distribution over the plasma cross section, since, the radial distribution of atomic concentration in the jet is practically homogeneous at all plasma diameters under consideration ($50 \mu\text{m} \leq \varnothing_{pl} \leq 400 \mu\text{m}$) as it can be seen in Fig. 2. The homogeneity of the temperature distribution, in turn, is explained by the radiative type of thermal energy loss of plasma consisting of multi-electron atoms/ions.

The discovered homogeneity of the temperature distribution is explained by the radiative type of the thermal energy loss from a dense plasma consisting of multi-electron atoms/ions. In contrast to the transport losses (heat conductivity, diffusion), which lead to the formation

of temperature and particle density gradients from the periphery to the center of the plasma and, as a consequence, to outward flows of heat and matter, the radiation losses are local, i.e., each elementary volume of the plasma emits independently in accordance with its local temperature. In addition, the radiation power is strongly temperature dependent (e.g., the radiation power of the equilibrium plasma $\sim T^4$), so that even a relatively small inhomogeneity in the plasma temperature would cause a substantial change in the power of the local radiation. The radiation type of plasma energy balance leads not only to the temperature equalization over the plasma volume, but also to a certain

„thermostabilization“. The temperature of such a plasma is mostly defined by its chemical composition, density, optical thickness, its equilibrium/nonequilibrium but not by the heating power.

Both in the present work and in [9], only the integrated over the plasma lifetime experimental values of the absorbed laser energy were considered. However, to obtain the absorption coefficient, instantaneous values of the laser radiation are needed instead. To introduce a necessary correction in the calculations, a hypothesis of hydrodynamic plasma outflow from the illuminated area has been used in [9]. To obtain more reliable data on the plasma parameters n_i , $\langle Z \rangle$, and T , the measurements of the laser light absorption in the laser-produced plasma with time resolution of ≈ 0.5 ns are planned

Funding

This study was carried out under the state assignment (No. 0040-2019-0001) and was partially supported by the Foundation for the Advancement of Theoretical Physics and Mathematics „BASIS“ (grant # 22-1-5-81-1).

Conflict of interest

The authors declare that they have no conflict of interest.

References

- [1] V.V. Zabrodskii, Yu.M. Zadiranov, S.G. Kalmykov, A.M. Mozharov, M.V. Petrenko, M.E. Sasin, R.P. Seisyan, *Tech. Phys. Lett.*, **40** (15), 668 (2014).
- [2] V.P. Belik, S.G. Kalmykov, A.M. Mozharov, M.V. Petrenko, M.E. Sasin. *Tech. Phys. Lett.*, **43** (11), 1001 (2017). DOI: 10.21883/PJTF.2017.22.45255.16957
- [3] P.S. Butorinov, Y.M. Zadiranov, S.Y. Zuev, S.G. Kalmykov, V.N. Polkovnikov, M.E. Sasin, N.I. Chkhalo. *Tech. Phys.*, **63** (10), 1507 (2018). DOI: 10.21883/JTF.2018.10.46501.2477
- [4] N.I. Chkhalo, N.N. Salashchenko. *AIP Adv.*, **3**, 082130 (2013).
- [5] N.I. Chkhalo, N.N. Salashchenko. *Proc. 2013 Int. Workshop on EUV and SXR Sources*. URL: <https://www.euvlitho.com/2013/S19.pdf>
- [6] I. Fomenkov. *Proc. 2018 Source Workshop*. URL: <https://www.euvlitho.com/2018/S1.pdf>
- [7] S. Kalmykov, P. Butorin, M. Sasin. *J. Appl. Phys.*, **126**, 103301 (2019).
- [8] N. Chkhalo, S. Garakhin, A. Lopatin, A. Nechay, A. Pestov, V. Polkovnikov, N. Salashchenko, N. Tsybin, S. Zuev. *AIP Adv.*, **8**, 105003 (2018).
- [9] S. Kalmykov, P. Butorin, M. Sasin, V. Zakharov. *J. Phys. D: Appl. Phys.*, **55**, 105203 (2022).
- [10] K. Fahy, P. Dunne, L. McKinney, G. O’Sullivan, E. Sokell, J. White, A. Aguilar, J.M. Pomeroy, J.N. Tan, B. Blagojevic, E.-O. LeBigot, J.D. Gillaspay. *J. Phys. D: Appl. Phys.*, **37**, 3225 (2004). DOI: 10.1088/0022-3727/37/23/003
- [11] W. Lochte-Holtgreven. *Plasma Diagnostics*, 1st ed. (North-Holland/Wiley, 1968).
- [12] H.R. Griem. *Plasma Spectroscopy*, 1st ed. (McGraw-Hill, 1964).
- [13] A.V. Garbaruk, M.S. Gritskevich, S.G. Kalmykov, A.M. Mozharov, M.E. Sasin. *J. Phys. D: Appl. Phys.*, **50**, 025201 (2017). DOI: 10.1088/1361-6463/50/2/025201
- [14] A.V. Garbaruk, D.A. Demidov, S.G. Kalmykov, M.E. Sasin. *Zh. Tekh. Fiz.*, **81** (6), 20 (2011).
- [15] A.V. Belashov, P.S. Butorin, Yu.M. Zadiranov, S.G. Kalmykov, V.A. Maximov, M.E. Sasin, P.Yu. Serdobintsev. *Opt. Spectrosc.*, **128**, 1328–1331 (2020). DOI: 10.1134/S0030400X2008007X
- [16] Y.P. Raizer. *Gas Discharge Physics* (Springer, Berlin, 1991), p. 33–51.

Translated by D.Safin